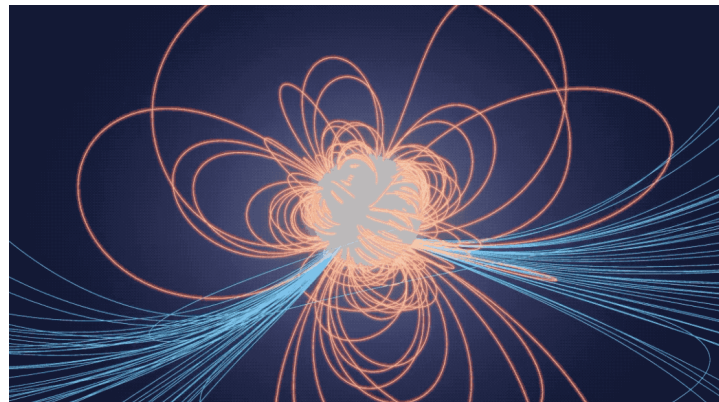

Constraining the neutron stars equation of state with NICER



LINA ISSA

15 avril 2021 - 15 août 2021

Under the supervision of NATALIE WEBB

Je soussignée Lina Issa certifie sur l'honneur :

1. que les résultats décrits dans ce rapport sont l'aboutissement de mon travail;
2. que je suis l'auteure de ce rapport;
3. que je n'ai pas utilisé des sources ou résultats tiers sans clairement les citer et les référencer selon les règles bibliographiques préconisées.

Je déclare que ce travail ne peut être suspecté de plagiat

Date: 22/06/2021

Abstract

Pulsars are typically studied in the radio domain, but studying them at higher energies allows us resolve features on the surface as small as a kilometre, as well as accurately measure their radii, which are of the order of 12 km. We study the X-ray radiation of thermally emitting pulsars detected by the NASA mission NICER (Neutron Star Interior Composition Explorer), installed on the International Space Station since 2017, to probe both the neutron stars' interior and exterior. In particular, we reduce and analyse the NICER X-ray spectral-timing event data of one chosen pulsar with a fairly low magnetic field and for which an accurate mass measurement from radio observations has already been determined. We perform pulse profile modelling for the pulsar to extract the waveform and subsequently compare it to cutting-edge relativistic models (Riley et al. 2019) that take into account relativistic effects on the emitted radiation assuming a model for the surface emission. Then, a Bayesian inference is applied on our data sets to retrieve parameters such as the mass and the equatorial radius. Knowing the mass and the radius allows us to constrain the density and pressure of the pulsating neutron star and thus to have a better understanding of the material making up its core and of the equation of state of dense matter. Finally, we infer the shape and location of the emitting region, providing us with an insight into the magnetic configuration of the pulsating neutron star. Comparing the radio and X-ray light curves also allows us to infer the site of the radio emission.

Contents

Abstract	3
 1 Introduction : the neutron stars under scrutiny with <i>NICER</i>	1
1.1 The make-up of neutron stars	1
1.2 The different populations of neutron stars	3
1.3 The <i>NICER</i> telescope: unveiling neutron stars' interiors	6
 2 Modelling the X-ray emission from MPS_s surface hot spots	10
2.1 The emission models of pulsar	10
2.2 The Pulse profile modelling technique with a Bayesian approach	13
2.3 M , R and EOS inference with XPSI	14
 3 The study of one millisecond pulsar: PSR J0030+0451	15
3.1 Pulse profile analysis of PSR J0030+0451	15
3.2 Post-Processing results	16
 Conclusion and Perspectives	18
 References	19

List of Figures

1	Structure of a neutron star	2
2	EOS models and mass-radius relationship	3
3	Schematic illustration of a pulsar	4
4	$\dot{P} - P$ diagram of pulsars	5
5	Pulse profile of PSR+J0030	7
6	Light bending effect on pulses from neutron stars surface hot spots	8
7	Illustration of the magnetosphere structure around a pulsar	11
8	Spectrum of PSR B0656+14	12
9	2D phasogram of synthetic data	13
10	Posterior expected signal of PSR J0030+0451	15
11	M and R inference	16
12	Posterior density estimation of the model parameters	17

1 Introduction : the neutron stars under scrutiny with NICER

Neutron stars are some of the most exotic objects in the Universe. Indeed, with a mass of roughly one solar mass contained in a sphere of about 10 km radius, the size of any big city, they challenge our understanding of matter in an extremely dense and cold environment [1] [2]. One way to quantify how compact these objects are is through *the compactness parameter*, also called the *relativity parameter* defined as a relation between the gravitational mass M of an object, its radius R , the gravitational constant G and the speed of light c as follows:

$$\Xi = \frac{GM}{Rc^2} \quad (1.1)$$

Neutron stars' compactness is about $\Xi \sim 0.2$, while that of a sun like star is 2×10^{-6} , and that of a black hole is 1, which sets the limit that an astrophysical object can reach.

Neutron stars are believed to be the leftovers of massive stars that exploded in a core-collapse supernovae [3]. In this scenario, the iron core of the dying star collapses into a very dense object, reaching ten times the density of an atomic nucleus, $\rho > 10^{14} \text{ g/cm}^3$. Before the supernova explosion, the intern structure of the dying star is stratified, the lightest elements being in the outer shells. The iron core is supported against gravitational collapse by the electronic degeneracy pressure as long as its mass does not exceed the Chandrasekhar mass¹. However, this balance is challenged by the neutronisation of the nuclei through electronic capture² occurring when matter is compressed at such high densities. This leads to a depletion of electrons and, *in fine*, to a decrease of the electronic degeneracy pressure: the core is no longer supported against gravity and collapses until it reaches the atomic density : a neutron star is born.

After briefly depicting their structure, we will investigate the different populations of neutron stars in terms of their observational properties. Then, we show how one can take advantage of these to probe their interior. We will put a particular emphasis on the NASA Space Observatory NICER³[5], an X-ray telescope launched in 2017 and installed on the International Space Station.

1.1 The make-up of neutron stars

The neutron star's structure can be broken down into 4 layers, with the density getting higher with depth, as shown in FIGURE 1:

- i) **the atmosphere:** the surface of neutron stars is surrounded by a thin (about 10 cm)[6] atmosphere only composed of hydrogen⁴.
- ii) **the envelope or surface:** below the atmosphere, an envelope of heavier elements with a stratified structure lies on the crust. As we go deeper in the envelope, the elements become more massive, up to the iron on its boundary with the crust. The density and the pressure are high enough for the nuclei to be fully ionised and for the electrons to be degenerate. The matter is well described as a fully ionised plasma embedded in a sea of degenerate free electrons.

¹The Chandrasekar mass is the maximum mass of a star supported against collapse by the electronic degeneracy pressure [4].

² $p + e^- \rightarrow n + \nu_e$

³Neutron Star Interior Composition Explorer

⁴If the neutron star has accreted matter from a companion star, there can also be found other light elements such as helium or carbon deep in the atmosphere.

- iii) **the crust:** The density in the crust reaches a density as high as $\rho \geq 10^9 \text{ g/cm}^3$ [7], so that the neutronisation of the nuclei takes place, in which protons are converted into neutrons by electronic capture. As a result, the nuclei become more massive with depth, increasing thus the density. Once the neutron-drip density is reached, which is about $\rho_{\text{drip}} \sim 10^{11} \text{ g/cm}^3$, the neutralisation is halted and the neutrons are liberated from their nuclei. The free neutrons are believed to be in a superfluid state. In the crust, the neutron-rich nuclei are arranged into a crystal lattice, bound together by Coulomb interaction and immersed in a sea of superfluid neutrons. As we go deeper in the crust, the density increases and the free neutrons contribute increasingly to the pressure.
- iv) **the core :** The outer core harbours a mixture of superconductive protons and superfluid neutrons. Indeed, once the nuclear density is reached, individual nuclei can no longer exist and dissolve to form a neutron-rich nucleonic matter. The mean distance between particles being about the Fermi distance⁵, neutrons can interact by the nuclear force, which becomes the dominant source of pressure. As for the inner part of the core, its composition is yet to be fully understood. Indeed, the behaviour of the matter under such extreme conditions is hardly reproduced on Earth, leaving the issue open for theoretical suggestions.

The microphysics of the dense matter interactions in neutron stars' core is macroscopically expressed through the equation of state of the star (hereafter EOS), that is a density-pressure-temperature relation. The EOS being highly sensitive to the make-up of the core, the uncertainties on its composition are translated into EOS uncertainties. As the temperature in neutron stars' core is nearly null, the dense and cold matter in the core of neutron stars can be safely described as a barotropic fluid, so that the EOS can be given as a relation between pressure and density only. Given the high compactness of neutron stars (see EQUATION1.1), their structure needs to be described in the framework of General Relativity. In that regime, the stellar structure equations are the Tolman-Oppenheimer-Volkoff (T.O.V) system[8] [9] given in EQUATION 1.2

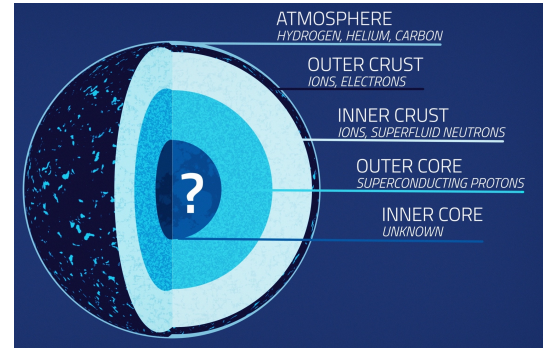


Figure 1: Credits: NASA's Goddard Space Flight Center/Conceptual Image Lab

$$\begin{aligned}
 \frac{dm}{dr} &= 4\pi r^2 \rho(r) \\
 \frac{dP}{dr} &= - \left(\rho(r) + \frac{P(r)}{c^2} \right) \frac{d\phi}{dr} \\
 \frac{d\phi}{dr} &= \frac{Gm(r)}{r^2} \left(1 - \frac{2Gm(r)}{rc^2} \right)^{-1} \left(1 + 4\pi \frac{P(r)r^3}{m(r)c^2} \right)
 \end{aligned} \tag{1.2}$$

where ϕ is the gravitational field, G the gravitational constant, m the mass of a sphere with a radius r , P the pressure and ρ the density, both evaluated at r . This system describes the hydrodynamic equilibrium of a static⁶ non-magnetic and relativistic object⁷. To solve this system one needs to consider an EOS, that is $P(\rho)$ in order to determine the whole structure of the neutron star. This will give a maximum mass as illustrated in FIGURE 2 beyond which there is

⁵The fermi distance corresponds to $1 \text{ fm} = 10^{-15} \text{ m}$

⁶This assumption enforces a spacetime with spherical symmetry.

⁷For highly rotating and magnetised neutron stars, the T.O.V needs to be amended [10].

no stable solution and the object collapses into a black hole. Thus, by measuring the mass of a neutron star, one can rule out any EOS models for which the measured mass M is greater than the maximum mass predicted by the EOS model M_{\max} : $M_{\max, \text{EOS}} < M$.

There are different families of EOS models suggested for the interior of neutron stars. The traditional one, gathered under the name of nucleonic models, describes the inner core as mostly filled with neutrons. Other models include strange quarks, either in the form of deconfined quark mixture, as in quark star models, or in an exotic particle such as hyperons (strange baryon), as in hybrid star models. These three families of models are represented in a density-pressure plane in FIGURE 2. Together with the T.O.V system, an EOS model yields to a mass-radius relation as illustrated in the right panel of FIGURE 2. Indeed, this relation is obtained by solving the T.O.V system with an EOS that closes the system and with a given central density and a spin rate [11]. The gravitational mass of a neutron star M can then be integrated to get a mass-radius relation assuming that the pressure is cancelled out at the radius R of the star.

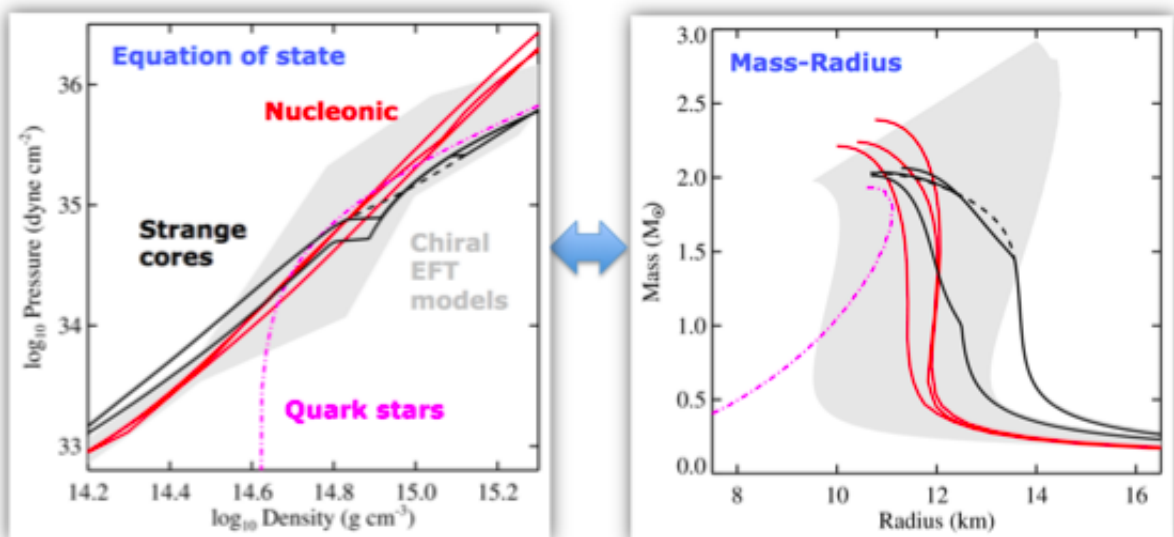


Figure 2: *Left panel:* Theoretical models of EOS obtained assuming a nucleonic core (in red), an hybrid model with strange quarks (in solid black) and a deconfined quark core (in purple). *Right panel:* The corresponding mass-radius relation for each EOS models is driven from the T.O.V system. For a given EOS model, there is a set of (M - R) couple values possible. Figure taken from [12]

1.2 The different populations of neutron stars

The classification of neutron stars is mostly based on their observational signatures. They are commonly separated into two classes, depending on the situation in which they are found: isolated or involved in a binary (or even multiple) system.

Isolated neutron stars

At the neutron stars' surface, the temperature can reach 100 000 K, so that their thermal emission peaks mainly in the soft X-ray band. Given their small size and the poor sensitivity of X-ray instruments, it is difficult to detect the thermal emission from cool, isolated neutron stars. Currently, this is only achieved for nearby neutron stars that are closer than roughly

500 pc⁸. Only a dozen of dim X-ray thermally emitting sources have been discovered to date. Hence, neutron stars would have been extremely hard to observe and to study, would it not have been for *the pulsar phenomena*.

Pulsars are neutron stars surrounded by a rotating magnetosphere, with a magnetic field about $10^{7\text{--}14}\text{G}$ and a rotational period ranging from about *unit1ms* up to roughly *unit1s*. The charged particles are accelerated along the open magnetic field lines and escape at the polar cap, leading to the emission of an energetic and focused beam, as illustrated in FIGURE 3. Since the magnetic field of the neutron star is not necessarily aligned with the rotational axis, an observer that happens to be along the line of sight of a beam will perceive a regularly pulsed signal, with a pulsation equating that of the rotational period of the neutron star. These energetic beams are mostly detected in the radio band but some of them are detected at higher energies, particularly in X and in gamma γ bands (see SECTION 2.1). The detection of a pulsar enables a distance measurement thanks to the dispersion effect that induces a delay in the arrival time of photons depending on their frequency.

Since a pulsar can be considered as a magnetic dipole, it loses energy by radiation which is extracted from its rotational reservoir⁹. As a result, the pulsar spins down and the period increases $\dot{P} > 0$: this is referred to as the *spin down law* (see EQUATION 1.3).

$$\begin{aligned} E_{\text{rot}} &= \frac{1}{2} I \Omega^2, \\ \dot{E}_{\text{rot}} &= -\dot{E}_{\text{rot}} = -4\pi^2 I \frac{\dot{P}}{P^3} \end{aligned} \tag{1.3}$$

with I the moment of inertia of the star, Ω its angular speed and P its period, with $P = 2\pi/\Omega$. Then, it is often assumed that the rotational speed evolution follows a power law

$$\dot{\Omega} = -k\Omega^\alpha \tag{1.4}$$

in which α is the braking index and k a coefficient.

The age of a pulsar can be deduced from the measurement of the spin down rate \dot{P} , assuming the power law evolution in (1.4). The observed pulsars with a known period, period derivative and magnetic field are represented in a $\dot{P} - P$ plane in FIGURE 4. From this diagram, it appears that the pulsars can be gathered into three groups:

⁸This only applies for cold and isolated pulsars. Magnetars, for example, can be detected as far as ~ 1 kpc due to their brightness

⁹assuming that the neutron star is old enough (older than hundred years). Otherwise, the rotation breaks the spherical symmetry by flattening the poles, generating gravitational waves radiation

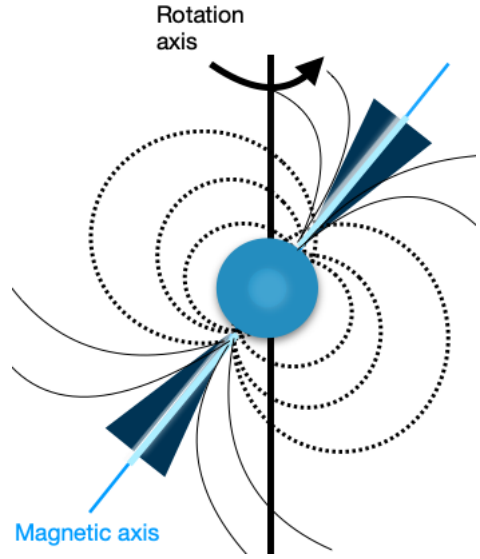


Figure 3: Schematic illustration of a pulsating neutron star with the magnetic field lines drawn in dashed and solid lines.

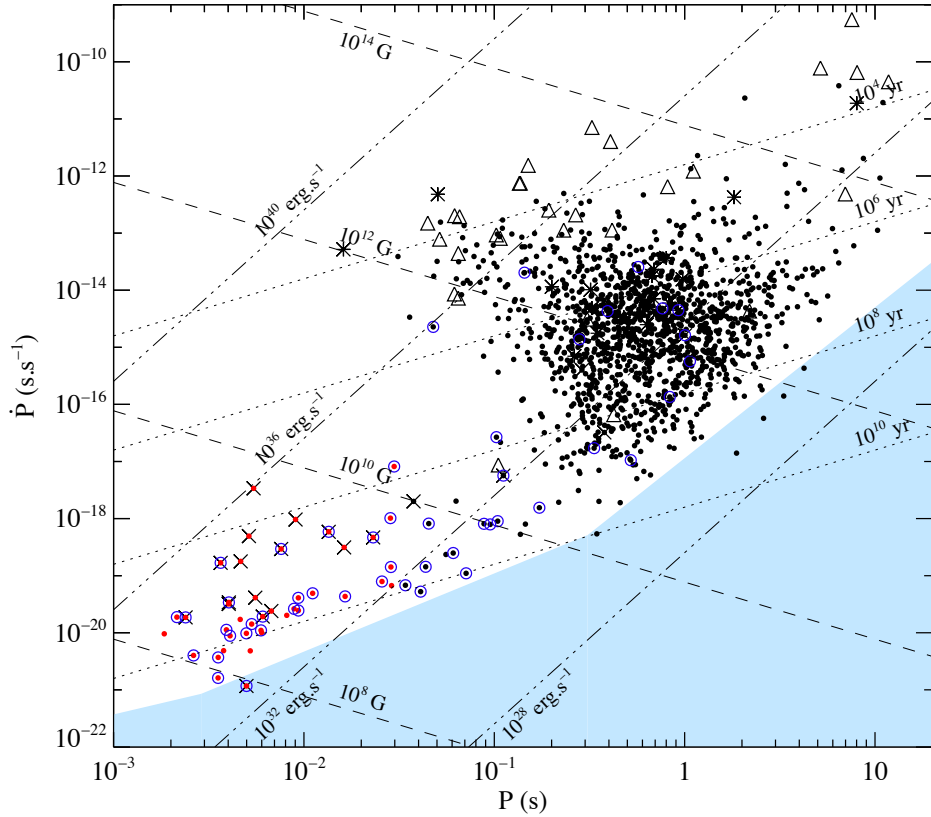


Figure 4: $\dot{P} - P$ diagram of observed pulsars. The pulsars are represented with a dot in a blue circle if they have been identified in a binary system, with a cross if in a globular cluster, as a star if extragalactic and as a triangle if associated with a supernova remnant. The pulsars in red have their period less than 30 ms: they belong to the millisecond pulsar class. The diagram also displays the lines of constant age (in dotted lines), of constant magnetic field (in dashed lines) and of energy loss (in dash-dotted lines). The blue shaded area is the graveyard delimited by the death line. Below that line, models predict that the radio emission is no longer sustained. Figure taken from [13]

- i) **"standard" pulsars:** This is the main population, with about 90% of the observed pulsars. Their period spans from $P \sim 30$ ms up to $P \sim 30$ s and their magnetic field ranges from 10^{11} to 10^{13} G.
- ii) **millisecond pulsars**, also known as recycled pulsars (hereafter MSP): These pulsars stand out for at least two reasons. First they spin up rapidly, their rotational period being in the order of the millisecond. Then, they are older than the standard pulsar population and have a lower magnetic field, about $B < 10^9$ G. This is well explained by the fact that these pulsars get spun up by the accretion from a companion star. This is corroborated by the fact that millisecond pulsars are very often found in a binary system ($\sim 80\%$) and around half of known MSPs are in globular clusters [14].
- iii) **magnetar:** This population of pulsars occupies the top right corner of the diagram (FIGURE 4). They stand out by their higher magnetic field, about 10^{14} G and a slower rotation, from $P \sim 6$ s to $P \sim 12$ s [15].

Neutron stars in a binary system

As for neutron stars involved in a binary system, other behaviours can be displayed. We differentiate neutron stars with a stellar companion from those with another compact object, such as another neutron star, a stellar-mass black hole or even a white dwarf. The former can

form an X-binary, while the latter is a source of gravitational waves. In an X-ray binary, the external layers of the companion star overflow the Roche lobe¹⁰ and fall through the inner Lagrangian point, where the gravitational force of the stars is cancelled, until it is captured by the compact object, forming an accretion disc around it, due to the excess of angular momentum from the rotation of the binary system. The thermally emitting disk in the X-rays helps to put constraints on the radius of the neutron star. If the companion is another compact object, the binary system loses orbital energy by gravitational waves radiation, leading in the final stage to the merger of the two objects. The neutron star involved in such a binary system is thus revealed to us with the release of gravitation waves, for inspiralling compact objects distort the space-time fabric, creating ripples that propagate at the speed of light. Then, the merger itself can be the source of a multi-wavelength signal, such as short gamma ray bursts, kilonovae and afterglows. Multi-messengers observations are a golden opportunity to study neutron stars since they can provide us with an unprecedented insight into their cores[16] [17].

1.3 The NICER telescope: unveiling neutron stars' interiors

The observation of various neutron stars helps improving our understanding of the dense matter in their core. Given the relation between the EOS and the mass-radius relation described in FIGURE 2, a mass-radius measurement amounts to inferring the core equation of state.

The mass measurement of a neutron star can put stringent constraints on the equation of state, ruling out those predicting a lower maximum mass than the one measured. The mass is usually determined in a binary system, from orbital parameters and the Kepler equations, which is done even more precisely if the neutron star is involved with another compact object. Those mass constraints are inferred by timing radio pulsars [18].

As for the radius measurement, this could be achieved, in principal, by investigating the spectral lines in the thermal emission from a neutron stars' surface. The compactness (see EQUATION 1.1), can be deduced from the gravitational redshift of the spectral lines¹¹ whose expression is given by EQUATION (1.5).

$$\frac{\lambda_{\text{measured}}}{\lambda_0} = 1 + z = \frac{1}{\sqrt{1 - 2 \times \Xi}} \quad (1.5)$$

where $\lambda_{\text{measured}}$ is the observed wavelength, λ_0 the rest-frame wavelength and z the redshift. One can also introduce the gravitational parameter g_r as $g_r = 1/(1+z)$.

Thus, knowing the gravitational redshift z can give access to the structure of the star. However, in practice, this has been proven to be quite infructuous given the various uncertainties that hinder such spectral analysis¹² [19]. Instead, one can take advantage of a transiently-accreting and X-ray bursting neutron star to perform a radius measurement via an X-ray spectral modelling. Indeed, when these bursts reach the Eddington flux, the gravitational mass of the neutron star can be retrieved knowing the distance of the source as well as the gravitational redshift [20].

¹⁰From the astronomer Edward Roche. It is the surface of equipotential of the binary system accounting both the gravitational and the centrifugal force.

¹¹To date, there has not been a confirmed observations of spectral lines in the thermal emission from the surface of neutron stars.

¹²More particularly, the measurement is highly model-dependant, so that it relies on different assumptions that are just as much source of uncertainties.

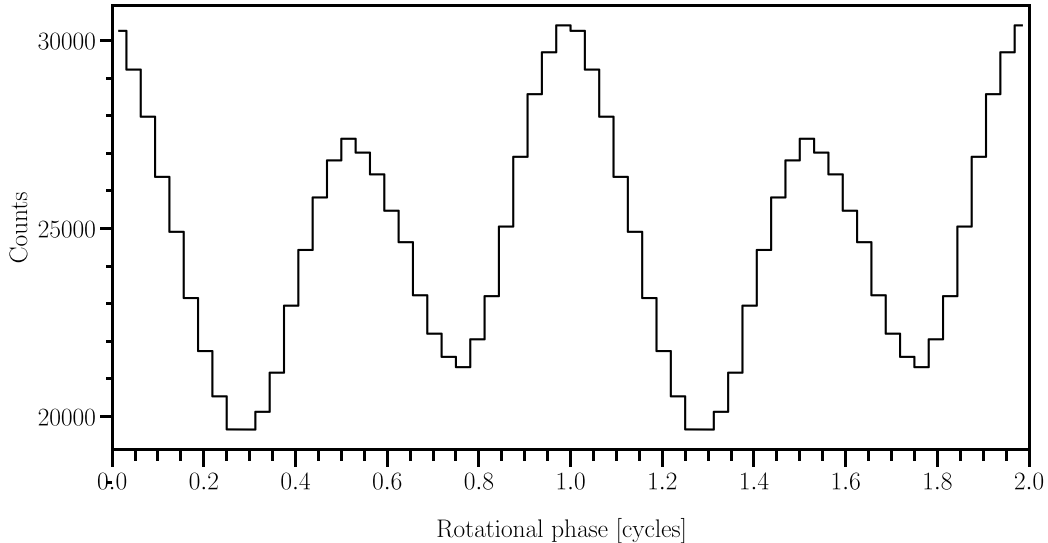


Figure 5: Pulse profile of PSR+J0030 obtained after phase folding the X-ray events detected by NICER [10]

There is another approach to measure the neutron stars' radius which involves the millisecond pulsars population. Indeed, as pointed out in FIGURE 4, the millisecond pulsars are characterized by a low magnetic field, and since they are older than the other pulsars, their surface is overall colder ($T < 10^5$ K). Thus, their thermal emission in the X-ray arises mainly from small regions called *hot spots*. Those small emitting regions are revealed through phase-resolved X-ray observations by the presence of rotation-induced pulsations¹³. In FIGURE 5, we present an example of a pulse profile¹⁴ of the pulsar PSR J0030+0451 obtained by phase-folding X-ray events. Each observed pulsation can be associated to a hot spot. As displayed in FIGURE 6, the observed pulsation is modulated by light bending exerted by the neutron star, so that one can retrieve a relation between mass and radius by accurately measuring this relativistic effect in neutron stars' light curves. More particularly, the rapid spin of MPs, (> 100 Hz), ensures that there is enough detected pulsed photons and reduces the level of uncertainties on the mass and radius constraints [10].

Indeed, the spectra and light curves of the hot spots encode information about the mass and the radius of a neutron star in various ways, notably via gravitational effects. As shown in EQUATION 1.6, the gravitational redshift appears in the expression of the emergent radiation, F_ν , expressed at frequency $\nu = g_r \nu_0$, ν_0 being the emission frequency in the frame of the neutron star, and for an observer at a distance D from the star.

$$F_\nu = 2 \left(\frac{R}{D} \right)^2 g_r \int K I_{\nu_0}(\mu) \mu d\mu \quad (1.6)$$

with $\mu = \cos(\theta)$, where θ is the angle between the normal and wave vector of the emitting spot, I_ν the specific intensity and K a geometrical parameter depending on the shape of the hot spot [21].

For models including a neutron star's atmosphere[21], one can retrieve an additional information on the mass and radius ratio through the surface gravity g , defined in EQUATION 1.7, by investigating the frequency-dependent limb darkening effect which accounts for the

¹³These pulsations are not observed if the rotation axis of the neutron star is aligned with either the line of sight or the magnetic axis

¹⁴X-ray counts per rotational bins per channel counts of the detector

anisotropy of the emergent radiation and the energy-dependency of the light curves [6].

$$g = \frac{GM}{R^2}(1+z) \quad (1.7)$$

The NICER X-ray telescope is particularly well suited to carry out such kinds of studies. Launched in 2017, this soft X-ray telescope on board the International Space Station is able to perform X-ray timing and spectroscopy observations of pulsars[5]. It is composed of a lightweight X-ray concentrator optics operating in 0.2 – 12 keV and a small silicon drift detectors. NICER can time-stamp these X-rays with an absolute timing better than 300 ns, thus enabling a precise tracking of the pulsations from the most rapid neutron stars.

Its energy resolution is similar to that of *XMM-Newton* and Chandra, while its time resolution is about 100 to 1000 times better than that of XMM. Moreover, it stands out from other X-ray telescope by its greater sensitivity, the minimum detectable flux¹⁵ being about 3×10^{-14} ergs $s^{-1}cm^{-2}$ and with its spatial resolution about 5'' (non-imaging field of view), slightly better than XMM. It can also accumulate up to 2 Ms of observations, way more than the ~ 100 ks of Chandra's or XMM 's observations. It has an effective area of 0.2 m² at 2 keV dropping to 0.06 m² at 6 keV [5]. The high energy resolution of NICER enables phase-resolved spectroscopy, while the absolute time stamps allow coherent light curves integration over years.

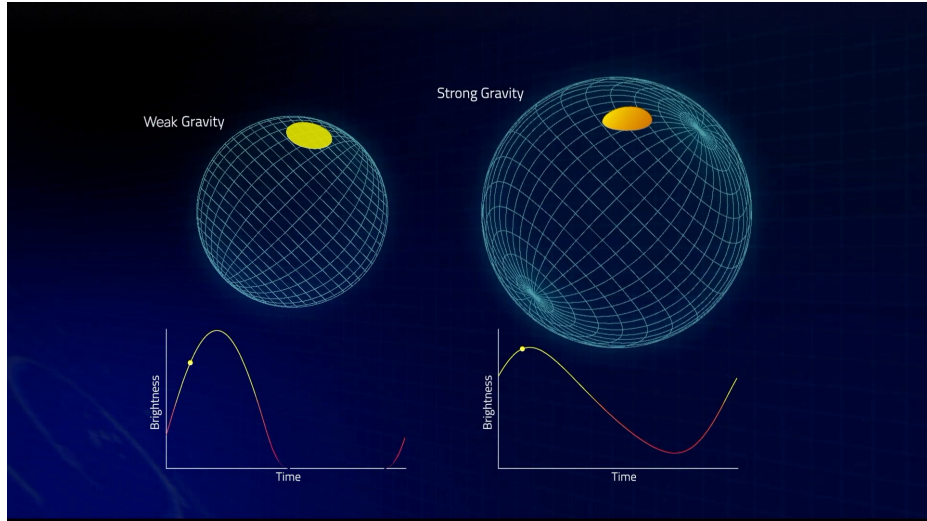


Figure 6: Pulses from neutron stars surface hot spots are subjected to the gravitational light bending. For a non-relativistic star, that is for a $\Xi \geq 10^{-4}$ (see EQUATION 1.1), when the emitting region goes out of view, the flux drops to zero. That is not the case for a neutron stars whose great gravity warps the spacetime in its vicinity.Credit: S. Morsink & NASA

All these characteristics combined make NICER the most suitable mission for the observation of pulsations in neutron stars' light curves.

Further analysis of these pulsations can provide us with information about i) the structure, ii) the dynamics [22], iii) the radiation pattern and subsequently the magnetic configuration of neutron stars. Indeed, the neutron star's radius can be derived from lighcurves analysis (see SECTION 2.2), while its mass can be inferred from phase coherent timing and then cross-checked with radio timing analysis if radio data is made available.

¹⁵In the 0.5 – 10 keV band. The minimum flux detectable is evaluated with a 5σ

One interesting target for NICER is the population of rotation-powered millisecond pulsars¹⁶. In a rotation-powered pulsar, the pulsations are extremely stable ($dP/dt \sim 10^{-18} - 10^{-21}$ [23]) in contrast with what is observed in an accretion-powered pulsar, for which the pulse profile variations are induced by changes in the accretion flows [24].

¹⁶In a rotation-powered pulsar, the radiation is powered by the loss in rotational energy, by opposition with an accretion-powered pulsar

2 Modelling the X-ray thermal emission of millisecond pulsars with XPSI

As mentioned above, rotation-powered MPs are the most suitable target to conduct pulse profile analysis on the rotationally-modulated emission from neutron stars surface hot spots. Hence, in this section and the following (SECTION 3), we will focus mainly on this population of millisecond pulsars.

Thanks to its large effective area of several square meters and its high time resolution, the NICER telescope can perform pulse profile modelling on the X-ray thermal emission from MPS hot spots surface. Before discussing the pulse profile technique, we ought to describe the physical processes at the origin of X-ray emission first. Then, we illustrate how the pulse profile analysis (SECTION 2.2), also known as waveform or light curve modelling, can be used to deliver simultaneous measurements of both the radius and the mass following a Bayesian approach (SECTION 2.3). We will introduce the X-Ray Pulsation Simulation and Inference (X-PSI), a software developed by Riley and described in [10] to carry out Bayesian modelling of X-ray pulsations detected by the NICER telescope.

2.1 The emission models of pulsar

The pulsar phenomenon is well described when we consider a neutron star as a magnetic dipole rotating in a dense magnetosphere as firstly assumed in the Goldreich & Julian's model [25] in which charged particles are stripped away from the surface, and with its magnetic axis not being aligned with the rotational axis (see FIGURE 3).

There are different non-thermal processes at work in the magnetosphere which can account for the emission of a multi-wavelength signal, from the radio band up to γ (Gev). Since the charged particles are trapped along the magnetic field lines, they can be accelerated and emit an electromagnetic signal via synchrotron/cyclotron or curvature mechanisms. There is also another mechanism at play contributing to the emergent radiation: the inverse Compton scattering. Indeed, the thermal X-ray emerging from the pulsar surface is scattered by the particles in the magnetosphere, producing energetic photons at even higher energies. All these processes produce a power-law spectrum, that is $P(\nu) \propto \nu^\alpha$. An important feature of the radio emission is that it must be produced by coherent processes. This might be achieved by a maser or by a coherent curvature radiation taking place in the pair production plasma above the polar cap [26].

To produce a radiation, the charged particles taken from the surface to the magnetosphere must be accelerated along the magnetic field lines.

This acceleration process is thought to happen in three regions :

- i) **the polar cap:** The polar cap is a region close to the surface delimited by the last open field line on the surface of the pulsar. The charged particles emit electromagnetic radiation via synchrotron-curvature mechanism and can emit very energetic, up to γ photons by inverse Compton scattering of the thermally emitted X photons from the pulsar surface. These high energy photons are absorbed through pair production mainly by interaction with the magnetic field: $\gamma B \rightarrow e^+e^-$. This leads to a cutoff at relatively low energy (\sim GeV) [28]. These newly formed charged particles are in turn accelerated and emit via the same mechanisms: synchrotron, curvature and inverse Compton scattering. The produced photons can in turn be absorbed by a pair production and so on. An electromagnetic cascade with a broad range of spectrum, from radio up to γ is developed in a focused beam.
- ii) **the slot gap:** The slot gap is a thin layer extending for several stellar radii along the boundary of closed magnetosphere. Compared to the polar cap, the acceleration of the charged particles can occur at higher latitudes, resulting in broader emission pulse [29]. The cutoff is mostly attributed to the finite energy of the emitting particles.
- iii) **the outer gap:** The outer gap is located close to the light cylinder, at low latitudes. Given that the magnetic field is lower in the outer gap than in the polar cap, the pair production is no more predominantly occurring by interaction with the magnetic field, but is mostly driven by photon collisions : $\gamma\gamma \rightarrow e^+e^-$. As a result, the cutoff in the outer gap is expected to occur at higher energies (> 10 GeV) than in the polar cap.

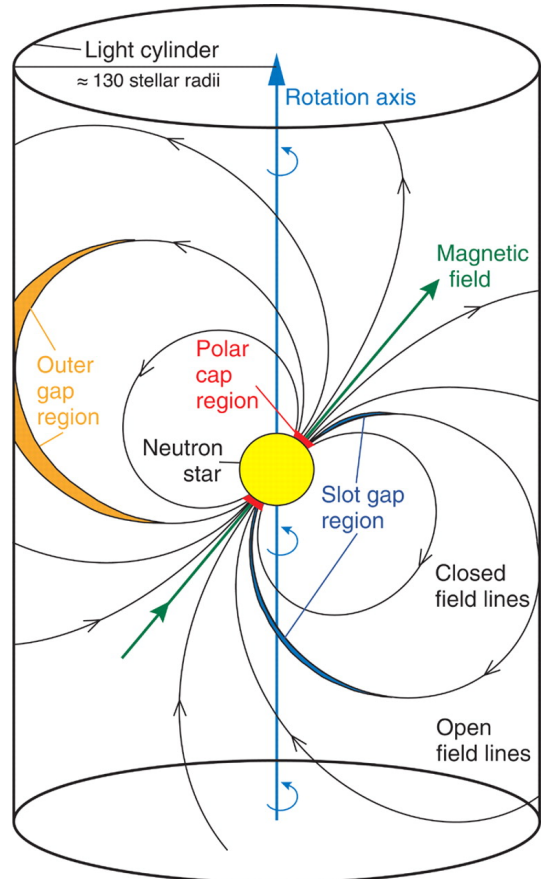


Figure 7: Illustration of the magnetosphere structure around a pulsar with the different emitting regions in which charged particles are accelerated. The light cylinder defines a critical surface which radius is $R_L = c/\Omega$ relatively to the rotational axis. Beyond that radius, the magnetic field lines crossing the light cylinder open and the charged particles can escape. Figure taken from [27]

Besides the non-thermal emission exposed above, there is a thermal component in the spectrum of a pulsar. As a result, different processes contribute to the emission in the X-ray luminosity of rotation-powered MPSs as illustrated in the spectrum of a pulsar given in FIGURE 8. The non-thermal emission is indicated by a power-law, while a blackbody like¹⁷ is indicative of a thermal emission from the surface. The observed non-thermal component in the X-ray can be attributed to the inverse Compton scattering of thermal photons from the surface, or to the synchrotron process in the polar cap that can produce radiation up to the X-rays. It can also originate not from the pulsar itself but from a pulsar wind or a synchrotron nebula which both produce a non-thermal unpulsed emission in the X band[23].

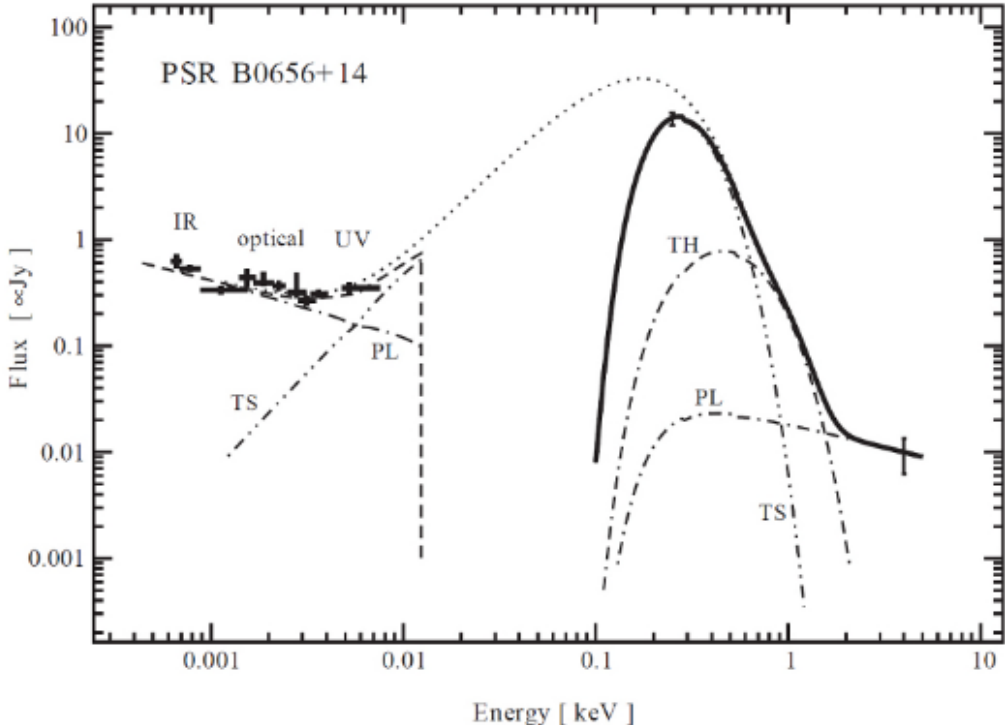


Figure 8: Spectra of a pulsar a young radio pulsar PSR B0656+14 with its thermal and non thermal components. The X-band is composed of a thermal soft component (TS), a thermal hard component (TH) and a non-thermal component represented as a power-law (PL). At lower energies, the spectrum is dominated by non thermal emission related to the magnetosphere activity. Figure taken from [30]

The thermal component is mainly in the X-ray band and stems from the small regions around the NS magnetic poles that are heated by the back-flow of relativistic particles that have been accelerated in the magnetosphere. Those regions in which energy from magnetospheric currents is deposited are known as *hot spots*. The expected temperatures and luminosities of the hot spots are[28] : $T_{\text{hot spot}} \sim 5 \times 10^5 - 5 \times 10^6 \text{ K}$ and $L_{\text{hot spot}} \sim 10^{28}-10^{32} \text{ erg s}^{-1}$. Their characteristics and shapes remain elusive but can be prospected with pulse profile modelling.

¹⁷The observed thermal emission differs from that of a blackbody because of the atmosphere which a source of anisotropy [21].

2.2 The Pulse profile modelling technique with a Bayesian approach

The pulse profile modelling exploits the light bending effect described in SECTION 1.3 to retrieve the compactness which is a ratio between the mass and the radius of the neutron star and to put constraints on the emitting regions, by investigating the depth of modulation and the harmonic content revealed in a phasogram, e.g. photons counts by rotational phase (see FIGURE 5 as an illustration).

In order to retrieve the mass and the radius of a rotationally powered MPS, one needs to know how the hot spots light curves depend on mass and radius. This can be achieved by fitting various parametrized light curve models to data using either a Bayesian approach or a Markov Chain Monte Carlo sampling methods [31]. However, those models need to take into account various assumptions about the geometry of the surface emission, such as the observer's inclination, the temperature pattern of the surface, and must be coupled to an atmosphere model in order to predict light curves for a given space-time structure governed by the mass, the radius and the spin rate of the pulsar. Only then can we infer, after having sampled those light curve predictions, pulsar mass and radius.

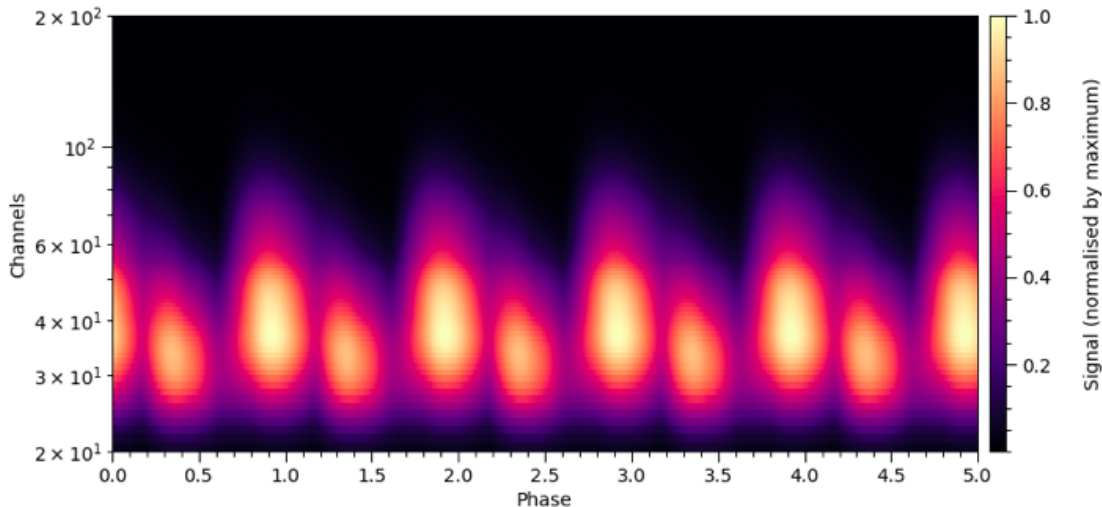


Figure 9: 2D phasogram of synthetic data. The data has been generated with two non-identical single-temperature hot spots.

The pulse profile technique starts with a light curve data that consists in an X-ray photon counts binned by energy channel and by rotational phase, as in the two-dimensional phasogram displayed in FIGURE 9 where we present a synthetic data as could be observed by NICER. The photon counts are binned by rotational phase and by energy channels scaling from 0.2 to 2 keV.

Then, an instrument response function including a Redistribution Matrix File and an Auxiliary Response File is applied to the data in order to convert the detectors channel into energy and to account for the efficiency of the detector. The pulse profile modelling relies on a parametrized light curve model describing the pulsations produced by a rotating, radiating surface from a relativistic pulsar. This model includes various sets of parameters setting up the geometry of the hot spots and the space-time structure.

In a Bayesian approach, a set of prior distributions is provided for those parameters. A likelihood evaluation is performed on the data for a given model with a given set of parameters. This gives the probability of obtaining the data from a given model. The likelihood calculation is then coupled to a sampler that explores parameter space to generate a posterior probability

distribution of those parameters. The equation of state inference can be either done directly if the equation of state parameters have been implemented in the model of light curves or can be derived using the mass and radius posteriors. The latter is based on the assumption that the likelihood function is proportional to the distribution of the mass and the radius, provided that the prior distribution of these two parameters are non-informative.

2.3 M , R and EOS inference with XPSI

The X-Ray Pulsation Simulation and Inference (X-PSI) is a Python software dedicated to performing a Pulse Profile modelling on the thermally emitted X-ray from hot regions on a rotating surface of an isolated pulsar¹⁸. The X-ray pulsation model is based on a likelihood functionality. Coupled to an open-source statistical sampling software such as MultiNest to be used in high-performance computing systems, it can draw samples from a Bayesian posterior probability of the model parameters, conditional to the observed data.

To generate a synthetic pulse profile, the X-PSI code performs a relativistic ray-tracing of the emergent radiation from a mapped surface emission which is propagated through the exterior spacetime of a rapidly rotating relativistic object. The ray propagation is affected by relativistic effects such as gravitational light bending and gravitational redshift as described in SECTION 2.1.

X-PSI constructs the emergent signal by combining a pre-processed dataset to i) instrument model representing the instrumental response of NICER, ii) an interstellar model describing radiation-matter interaction processes that affect the surface radiation field from the hot spots during its propagation to the instrument and iii) a background model of the radiation incident on the instrument. Then, X-PSI constructs a star by defining its surface radiation field and the hot regions, its photosphere and its exterior space-time. The X-PSI inference code handles different models of hot spots. There are different configurations of shapes and temperature pattern that could be implemented. For example, two hot spots can be forced to be related by antipodal symmetry. This configuration is motivated by physical consideration of a dominantly centred-dipolar field which is translated into a symmetrical distribution of the heat on the surface [10]. In other models, the two hot spots can have unshared parameters so that their properties and location have independent values, with the exception however that the two regions don't overlap. Different temperature patterns and shapes can be considered for the two regions: one that includes a uniform single temperature for each spot of a circular, crescent or even ring shapes (centred or off-centred) and one with a double temperature model can be considered for a region in the shape of a crescent or a ring.

Then the constructed star with all its attributes (photosphere, hot regions configuration and space-time) and the signal are combined into a likelihood functionality which provides the probability of the data as a function of parameters. The model also includes a prior distribution of the parameters entering in the likelihood function. At this step of the waveform modelling, X-PSI can produce synthetic light curves for a given set of parameters. To derive the posterior probability distribution of the model parameters, the likelihood functionality is coupled to a sampler during the inference process.

¹⁸A documentation can be found in https://thomasedwardriley.github.io/xpsi/model_construction.html

3 The study of one millisecond pulsar: PSR J0030+0451

We give in this section preliminary results of the MPS radio pulsar PSR J0030+0451. This rotation-powered pulsar has been first observed as a radio pulsar by Lommen et al.(2000) [14], before being detected as an X-ray pulsar (Becker et al. 2000) [32]. This multi-wavelength observation has enabled a measurement of its distance, estimated to be of 325 ± 9 pc, and of its spin frequency, which is estimated to be 205 Hz (Arzoumanian et al. 2018) [33].

3.1 Pulse profile analysis of PSR J0030+0451

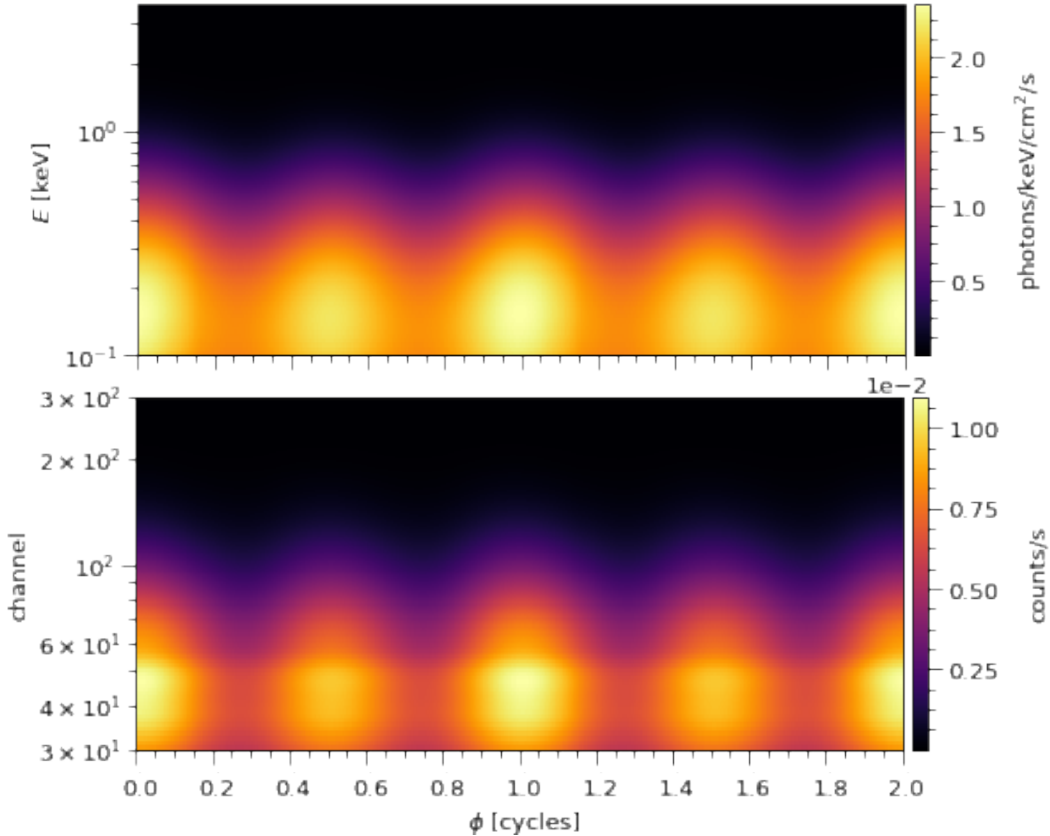


Figure 10: Posterior expected signal of PSR J0030+0451 for the Single Temperature Symmetric (STS) model. *On top*: The signal incident on the instrument, proportional to the specific photon flux. *On bottom* : The signal as detected by the detector with the instrumental response. The signal as perceived by NICER is slightly more constrained than the incident signal.

Since the observed light curve displayed in FIGURE 5 indicates the presence of two pulsations, we opt for a model including two hot spots. The analysis is undertaken for a simple model in which the two hot regions have been imposed to be at antipodal symmetry, with a single temperature for each one. The expected signal, taking into account the instrumental response and the propagation through the interstellar medium is presented in FIGURE 10. We have restricted the analysis to a subset of channel detectors [30, 300], corresponding to 0.3-3 eV and a total exposure time of 1936864.0 s.

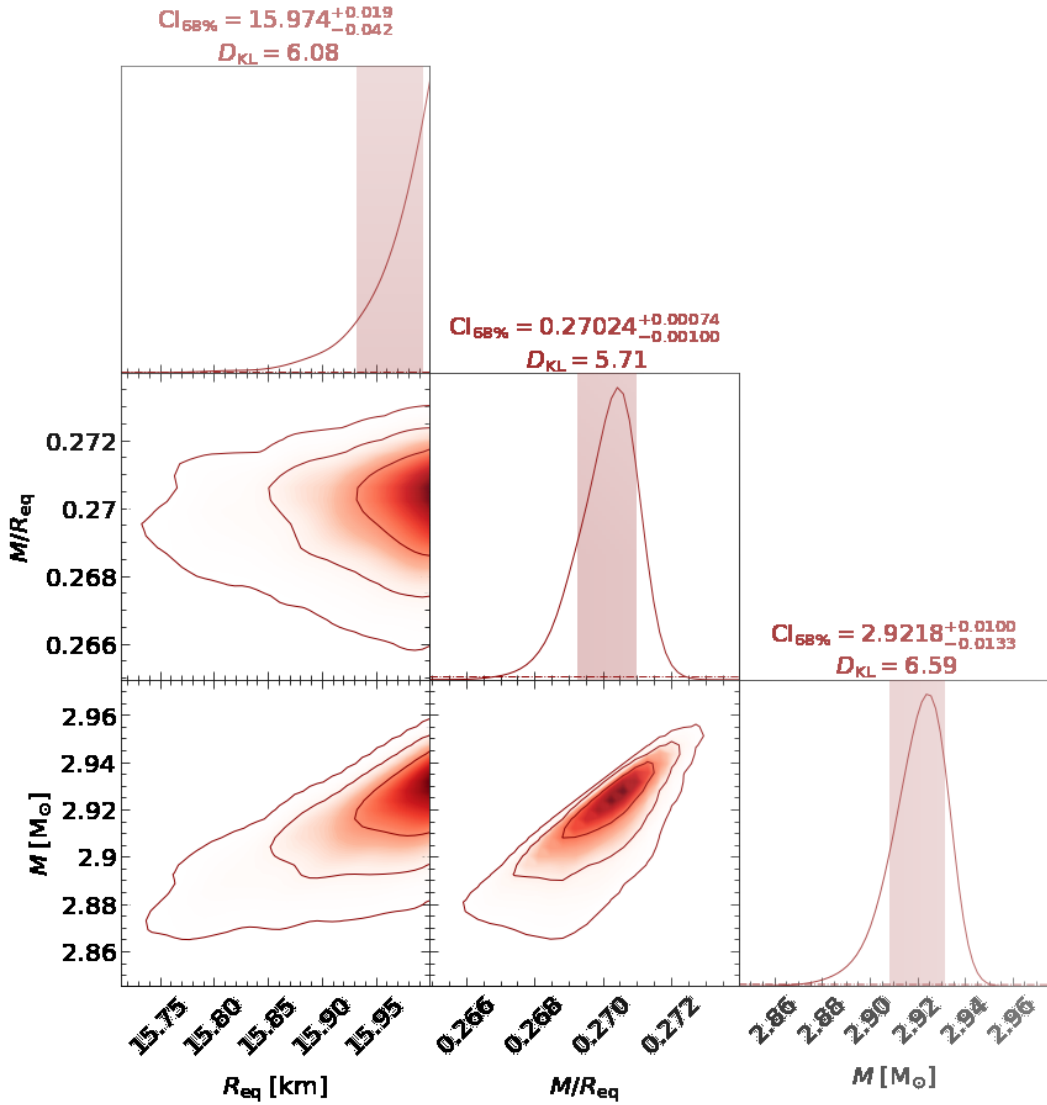


Figure 11: M and R Bayesian inference. The shaded area in top panels codes for the *credible interval*

3.2 Post-Processing results

In FIGURE 11, we represent the marginal posterior density distribution of the space-time structure parameters that are: the gravitational mass M , the equatorial radius R_{eq} and the compactness M/R_{eq} . STS model leads to an estimated equatorial radius of $R_{\text{eq}} \sim 15.974$ km and a gravitational mass of $M_{\text{grav}} \sim 2.9 M_{\odot}$. Those values are higher than expected and with respect to what is obtained with more sophisticated models of hot regions by Riley et al (2019)[10]. In the literature, the mass has been estimated to be $1.34 M_{\odot}$ and the radius to be 12.71 km.

The marginal density distribution for all the parameters of the model is displayed in FIGURE 12. Besides the space-time structure parameters, the marginal posterior density of geometric parameters of the hot regions are also represented. This result could, in principle, be used to infer the magnetic structure of the pulsar.

This Bayesian inference process described in this work is sensitive to model assumptions and leads to model-dependent results. In particular, it is based on strong atmosphere assumptions [19] and on the choice of the hot regions configuration [10].

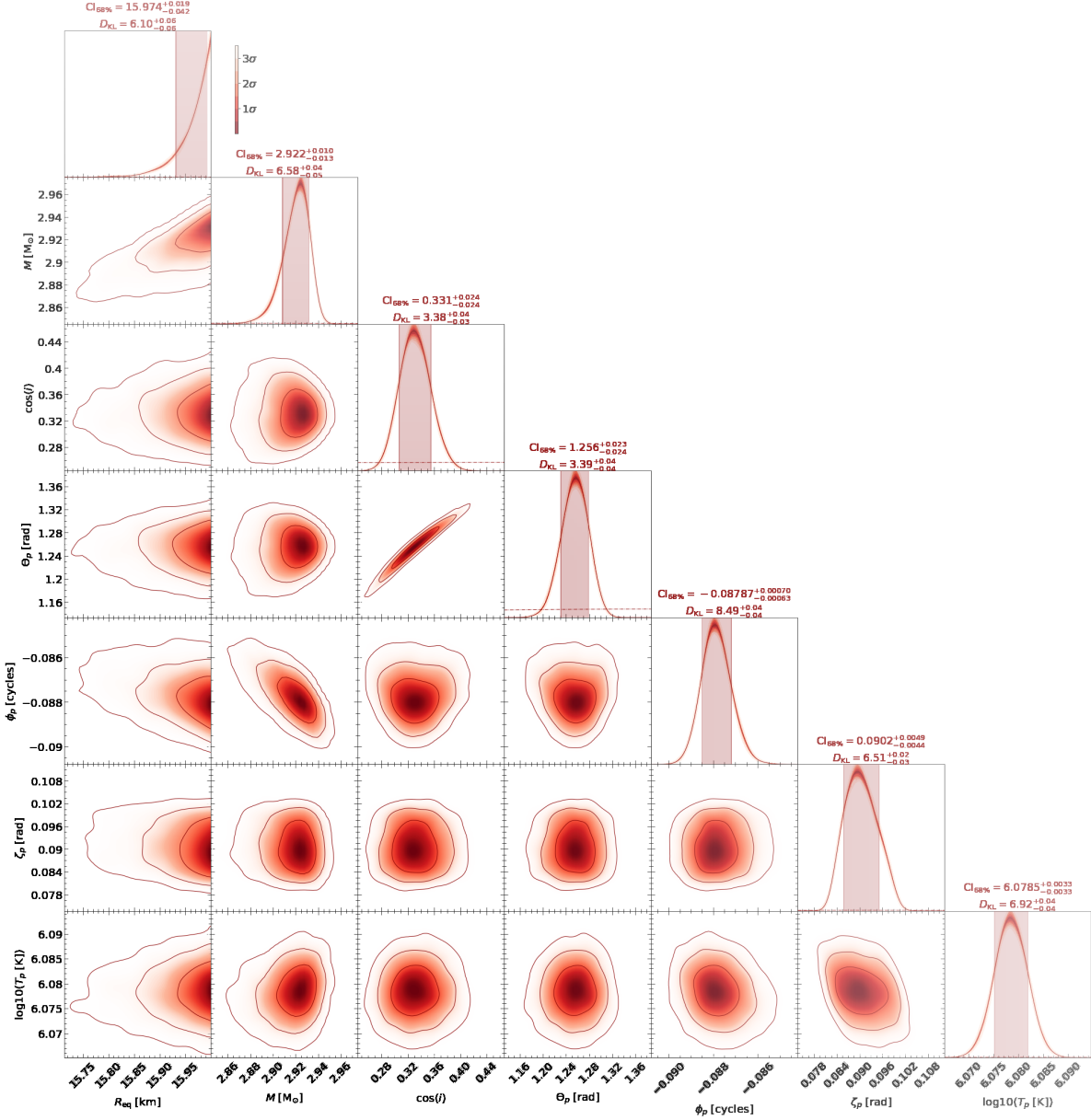


Figure 12: Posterior density estimation of the model parameters including geometrical parameters related to the hot spots geometry.

Conclusion and Perspectives

Conclusion We have conducted a preliminary Bayesian analysis on the rotation-powered millisecond pulsar PSR J0030+0451, using X-PSI, a likelihood-based software developed by Riley et al. (2019) and described in [10]. Further investigation on the parameters is mandatory to retrieve better constraints of the pulsar mass and radius. Indeed, the analysis relies on a simple model that imposes the two hot regions to be circular and symmetric. In the next step, we will try different hot spots configurations and compare the post processing results to deduce the best parameters constraints. It is possible that the large radius and mass found for PSR J0030+0451 is due to the model converging in a local minimum. Future studies will ensure that the whole of the parameter space is investigated in order to avoid this and provide a better estimate of the mass and the radius. Then, we will attempt to infer an EOS constraint. The study can be extended to other MPSs in order to get a wide sample of pulsars masses and radii and hence mapping the EOS.

Perspectives The pulse profile modelling technique described in SECTION 2.2 and used in this work does not only work for rotational powered pulsars. It can indeed be applied to the thermal X-ray pulsations from accretion-powered X-ray pulsars and from thermonuclear burst oscillation sources [24]. This will be at the heart of future X-ray timing missions such as the enhanced X-ray Timing and Polarimetry eXTP and the Spectroscopic Time-Resolving Observatory for Broadband Energy X-rays STROBE-X. The imaging X-ray telescope, Athena, a soft X-ray observatory, could also be used in a synergistic way for the pulse profile modelling provided by eXTP or STROBE-X.

Acknowledgements First of all, I would like to deeply thank my supervisor Natalie Webb for her constant support throughout the project and for her advices. I would also like to thank all the NICER people in Amstersdam, namely Riley, Devarshi, Yves Kini and of course Serena who have helped me to solve the numerous issues with the software. I obviously thank everyone in irap that I met: Erwan, Hugo, Quentin and Simon for sharing convivial coffee breaks with me, Benjamin for the laughs we shared in the office and Wilfried for his meticulous review of this work.

References

- [1] W. Baade and F. Zwicky, "On Supernovae," *Contributions from the Mount Wilson Observatory*, vol. 3, pp. 73–78, Jan. 1934.
- [2] I. S. Shklovsky, "On the Nature of the Source of X-Ray Emission of Sco XR-1.," *The Astrophysical Journal*, vol. 148, p. L1, Apr. 1967.
- [3] G. G. Pavlov, V. E. Zavlin, B. Aschenbach, J. Trümper, and D. Sanwal, "The Compact Central Object in Cassiopeia A: A Neutron Star with Hot Polar Caps or a Black Hole?," *The Astrophysical Journal*, vol. 531, pp. L53–L56, Mar. 2000.
- [4] S. Chandrasekhar, "Stellar Configurations with Degenerate Cores," *Journal of Astrophysics and Astronomy*, vol. 15, p. 133, June 1994.
- [5] K. Gendreau and Z. Arzoumanian, "Searching for a pulse," *Nature Astronomy*, vol. 1, pp. 895–895, Dec. 2017.
- [6] V. E. Zavlin and G. G. Pavlov, "Modeling Neutron Star Atmospheres," in *Neutron Stars, Pulsars, and Supernova Remnants* (W. Becker, H. Lesch, and J. Trümper, eds.), p. 263, Jan. 2002.
- [7] D. Page and S. Reddy, "Dense Matter in Compact Stars: Theoretical Developments and Observational Constraints," *Annual Review of Nuclear and Particle Science*, vol. 56, pp. 327–374, Nov. 2006.
- [8] J. R. Oppenheimer and G. M. Volkoff, "On Massive Neutron Cores," *Physical Review*, vol. 55, pp. 374–381, Feb. 1939.
- [9] N. K. Glendenning, *Compact stars. Nuclear physics, particle physics, and general relativity*. 1997.
- [10] T. E. Riley *et al.*, "A NICER View of PSR J0030+0451: Millisecond Pulsar Parameter Estimation," *The Astrophysical Journal Letters*, vol. 887, p. L21, Dec. 2019.
- [11] J. B. Hartle and K. S. Thorne, "Slowly Rotating Relativistic Stars. II. Models for Neutron Stars and Supermassive Stars," *The Astrophysical Journal*, vol. 153, p. 807, Sept. 1968.
- [12] A. Watts *et al.*, "Probing the neutron star interior and the Equation of State of cold dense matter with the SKA," in *Advancing Astrophysics with the Square Kilometre Array (AASKA14)*, p. 43, Apr. 2015.
- [13] J. H. Taylor and R. N. Manchester, "Recent observations of pulsars.," *Annual review of astronomy and astrophysics*, vol. 15, pp. 19–44, Jan. 1977.
- [14] D. R. Lorimer, "Binary and Millisecond Pulsars," *Living Reviews in Relativity*, vol. 11, p. 8, Nov. 2008.
- [15] S. Mereghetti, "The strongest cosmic magnets: soft gamma-ray repeaters and anomalous X-ray pulsars," *The Astronomy and Astrophysics Review*, vol. 15, pp. 225–287, July 2008.
- [16] H. Güven, K. Bozkurt, E. Khan, and J. Margueron, "Multimessenger and multiphysics Bayesian inference for the GW170817 binary neutron star merger," *PHYSICAL REVIEW C*, vol. 102, p. 015805, July 2020.
- [17] T. Dietrich *et al.*, "Multimessenger constraints on the neutron-star equation of state and the Hubble constant," *Science*, vol. 370, pp. 1450–1453, Dec. 2020.
- [18] J. M. Lattimer, "The Nuclear Equation of State and Neutron Star Masses," *Annual Review of Nuclear and Particle Science*, vol. 62, pp. 485–515, Nov. 2012.
- [19] S. Bogdanov *et al.*, "Constraints on Neutron Star Properties from X-Ray Observations of Millisecond Pulsars," *The Astrophysical Journal*, vol. 670, pp. 668–676, Nov. 2007.
- [20] N. Baillot d'Etivaux *et al.*, "New Constraints on the Nuclear Equation of State from the Thermal Emission of Neutron

- Stars in Quiescent Low-mass X-Ray Binaries," *The Astrophysical Journal*, vol. 887, p. 48, Dec. 2019.
- [21] V. E. Zavlin, Y. A. Shibanov, and G. G. Pavlov, "Effects of the gravitational field of a neutron star on the emission from hot polar spots on the surface of radio pulsars," *Astronomy Letters*, vol. 21, pp. 149–158, Mar. 1995.
- [22] A. L. Watts, "Thermonuclear Burst Oscillations," *Annual Review of Astron and Astrophys*, vol. 50, pp. 609–640, Sept. 2012.
- [23] W. Becker and J. Truemper, "The X-ray luminosity of rotation-powered neutron stars.,," *Astronomy and Astrophysics*, vol. 326, pp. 682–691, Oct. 1997.
- [24] A. L. Watts, "Constraining the neutron star equation of state using pulse profile modeling," in *Xiamen-CUSTIPEN Workshop on the Equation of State of Dense Neutron-Rich Matter in the Era of Gravitational Wave Astronomy*, vol. 2127 of *American Institute of Physics Conference Series*, p. 020008, July 2019.
- [25] P. Goldreich and W. H. Julian, "Pulsar Electrodynamics," *The Astrophysical Journal*, vol. 157, p. 869, Aug. 1969.
- [26] J. Dyks *et al.*, "The nature of pulsar radio emission," *Monthly Notices of the Royal Astronomical Society*, vol. 401, pp. 1781–1795, Jan. 2010.
- [27] E. Aliu and MAGIC Collaboration, "Observation of Pulsed γ -Rays Above 25 GeV from the Crab Pulsar with MAGIC," *Science*, vol. 322, p. 1221, Nov. 2008.
- [28] V. E. Zavlin and G. G. Pavlov, "Soft X-rays from polar caps of the millisecond pulsar J0437-4715," *Astronomy and Astrophysics*, vol. 329, pp. 583–598, Jan. 1998.
- [29] A. K. Harding, "Pulsar Physics and GLAST," in *The First GLAST Symposium* (S. Ritz, P. Michelson, and C. A. Meegan, eds.), vol. 921 of *American Institute of Physics Conference Series*, pp. 49–53, July 2007.
- [30] W. Becker, *X-Ray Emission from Pulsars and Neutron Stars*, vol. 357, p. 91. 2009.
- [31] M. C. Miller and F. K. Lamb, "Determining neutron star masses and radii via analysis of NICER energy-resolved waveform data," in *American Astronomical Society Meeting Abstracts #225*, vol. 225 of *American Astronomical Society Meeting Abstracts*, p. 214.09, Jan. 2015.
- [32] W. Becker, J. Trümper, A. N. Lommen, and D. C. Backer, "X-Rays from the Nearby Solitary Millisecond Pulsar PSR J0030+0451: The Final ROSAT Observations," *The Astrophysical Journal*, vol. 545, pp. 1015–1019, Dec. 2000.
- [33] Z. Arzoumanian, "NASA's Neutron star Interior Composition Explorer (NICER): mission overview and initial results," in *42nd COSPAR Scientific Assembly*, vol. 42, pp. E1.10–4–18, July 2018.